Physical Model for Understanding and Testing Long Range Prediction of Multipath Fading in Wireless Communications[*]

Hans Hallen*, **Shengquan Hu**[^] and **Alexandra Duel-Hallen**[+]

*Department of Physics, [+]Department of Electrical and Computer Engineering,
North Carolina State University, Raleigh, NC 27695
[^]Spreadtrum Communications Corp., Santa Clara, CA 95054

Abstract

Algorithms that enable adaptive transmission techniques on fading channels must reliably predict the wireless channel at least several milliseconds (a fraction of a wavelength) ahead. These long-range prediction (LRP) methods cannot be adequately tested with existing models. A novel, deterministic model is optimized for testing LRP methods since it: (1) *incorporates the physical variations* of the parameters associated with each reflector, which are not accounted for in stationary Rayleigh fading or Jakes model; (2) provides *quantitative limits* on the variation rate of these parameters for realistic fading environments, thus establishing tracking requirements for the LRP algorithm; (3) *identifies* the reflector *configurations* that will engender typical and challenging conditions for long range prediction algorithms, with insights not easily provided by ray-tracing or finite difference time domain methods; (4) creates *non-stationary* datasets to test such an algorithm; and (5) *illuminates the origins* of the temporal and statistical properties of measured data. It utilizes diffraction and can handle shadowing. We compare model data to outdoor microcell field measurements by examining their autocorrelation functions and probability density functions, and show that the insights are verified in prediction performance.

Keywords: realistic physical channel model, channel prediction, adaptive transmission, deterministic modeling, Rayleigh fading channel.

[*] Support for this work was provided by NSF grants CCR-9725271, CCR-9815002 and ARO grant DAAD 19-01-1-0638.

I. Introduction

The tremendous growth in demand for wireless communications capacity has created a need for new modulation, coding and detection methods that more efficiently use the multipath fading channels encountered in mobile radio. Since the channel changes rapidly, the transmitter and receiver are not usually optimized for current channel conditions, and thus fail to exploit the full potential of the wireless channel. New adaptive transmission techniques [1, 2] use both power and spectrum more efficiently to realize the higher bit rate transmission without sacrificing the Bit Error Rate (BER) performance. To implement these adaptive transmission methods in practice, *channel state information* (CSI) for a future block from tens to hundreds of data symbols long, a few msec for typical cellular signaling, must be available at the transmitter due to feedback delay and other constraints [1]. Significant degradation of performance results from using out-dated samples. Recently, we investigated a novel adaptive long-range fading channel prediction (LRP) algorithm [1, 3, 4, 5, 6, 7]. This method forecasts a wireless channel well beyond the coherence time, and provides enabling technology for adaptive transmission. In this paper, we describe a deterministic model that is specifically designed to provide insights and data sets to aid testing of LRP algorithms. The performance of such algorithms is limited by non-stationarity of the channel, so this property must be incorporated into the model in a physically realistic manner. We also require that the model be able to create typical or challenging test data sets, needed to investigate the average and limiting performance. We consider the channel to be a sum of sinusoidal waves, directly from the transmitter or after one reflection (single bounce approximation). The method of images, used to describe reflections, provides insights into the variation of Doppler frequency with mobile position – an important parameter variation. An augmentation with Fresnel diffraction makes the data sets realistic and yields insights into the variation of each wave's amplitude with position, the other important set of parameter variations. The insights allow us to create an environment and test data set that is typical or challenging for channel prediction. They solve the problem of choosing a meaningful reflector configuration and mobile route for testing the LRP method. The physical

model is primarily meant for outdoor systems where relatively large (10's of meters or more) distances from reflectors make our single-bounce approximation valid. The insights will remain valid in the indoor case, but multiple bounces will render the data sets produced by the model only qualitatively correct, since more waves will be important than are modeled in the single bounce approximation. If required, manual insertion of properly placed additional reflectors into the model allows generation of quantitatively correct indoor data.

Many models provide data sets for short-term fading. The deterministic, stationary *Jakes model* [8] is a standard model in computer simulations. The theoretical Rayleigh fading channel, in which the fading coefficients are modeled as complex Gaussian random variables [8, 9] can be used to set theoretical limits on performance. Various physical models [10] have been developed to either provide datasets or describe measurements. Statistical models overcome the variation of environments by assuming statistical variations (for a particular environment [11]) while providing an overall constraint such as time of arrival through placement on an ellipse [12], or clustering [13, 14]. While the statistical models do provide an adequate testbed for some systems, they often do not provide datasets that correspond to realistic physical variations in a particular environment (e.g, [15]) and their assumptions may not be applicable (e.g, [16]). For our primary goal of testing a long-range prediction algorithm, the non-stationary aspects of the channel, i.e. the variation of channel parameters (amplitudes, frequencies and phases) associated with each reflected wave must be properly modeled. The rate of change of these parameters significantly affects prediction accuracy [1, 3, 17, 18]. The key problem in modeling parameter variation is to do so in a physically meaningful way, which is not possible with the models described above. Our model does this by accurately accounting for the origins of the realistic physical variations, and providing insights to overcome the arbitrariness [16] of particular reflector placement. The LRP algorithm has similar performance on measured data and datasets generated by our model, whereas its performance using the Jakes model is significantly different [1, 3, 6, 17, 18].

In section II, we describe the physical model, computational details and its relation to other channel calculation methods. Section III contains a description of the model insights and their

origins, and section IV gives an overview of how these insights enhance our understanding of measured data channel statistics. The LRP algorithm and its performance is described in section V. Again, the insights are shown to correctly predict performance trends. We conclude in section VI.

II. The Physical Model

Our physical model for short-term fading differs considerably from propagation modeling studies [e.g, 19, 20] that consider long-term fading for base station siting or cell size. They average out the short-term fading, and typically rely on accurate environmental models to obtain quantitative agreement with measurements, although statistical factors have been used [21]. Our goal to test long-range prediction algorithms that forecast the channel to a fraction of a wavelength ahead implies that we need to predict the rapid channel variations associated with the short-term fading signal [8, 9]. Furthermore, the statistical properties of the test datasets, including the variations of the individual reflected wave amplitudes, frequencies, and phases need to be properly chosen. When we compare our model data to measured data, we do not compare it 'point-by-point.' Instead, we create datasets that have the same statistical properties. We show below that these statistics are influenced by the sizes and types, flat or curved, of the reflectors present, and that the performance of the LRP algorithm is also determined by these environmental properties. The lack of a point-by-point comparison is unusual in propagation studies [19]. Although we could arrange the reflectors in our study using an iterative procedure to produce point-by-point agreement, the result is unlikely to be unique unless a large amount of measured data is used. Furthermore, two tracks of short-term fading data for the mobile separated by a fraction of a wavelength will be quite different in general, if compared point-by-point. Their statistics, however, and the performance of the LRP algorithm on them will be similar. For algorithm verification, we also need to know if a dataset is going to be (statistically) typical for a mobile unit to encounter, or whether it represents a very challenging case that may rarely be encountered in practice. Our model provides these insights from theoretical considerations, not by repeated simulations [22], so that we can easily generate data of both types, and therefore make strong statements about the prediction algorithm performance in

any environment. We will consider just one resolved multipath component (*flat* fading). The use of the model for the frequency selective channel is discussed in [17].

The image method, upon which our physical model is based, can be used to calculate the exact electric field for a few specific geometries. We extend it for realistic objects with the use of apertures. Fresnel diffraction is required to maintain accuracy near the apertures [23]. Multiple scattering from small objects where diffraction is important creates an excessive number of image sources, and is the primary drawback of the method. This does not represent a serious deficiency, however, since the combination of imperfect reflection and rapid reduction of power with distance makes such multiply-diffracted signals weak compared to more direct waves – implying that all but a few of the image sources can be ignored. We ignore all but the first bounce in our model's automatic calculation. Besides, insights into the rates of parameter variations for each object producing a significant reflected wavefront can be readily deduced from the image method. The prediction only requires a local model of the flat fading, so even cases for which a weak diffracted signal serves as the source, such as a canyon-like street, can be accurately considered with this method. A few other methods can be used to produce data sets with proper non-stationary statistics. They involve calculation of the electric field in explicitly-defined environments. Finite difference time domain (FDTD) methods [19, 24] can be used more easily in complex environments, but for the purpose of these studies, we value the insights and generic prediction requirements of our model. A combination of ray tracing for long-term fading and identification of the few important rays, (effective transmitters in our notation) as in Ref. [25], with our method for local insights provides a complete simulation tool.

The augmentation of the image method for calculation of the microwave fields near realistic objects is accomplished by the addition of an aperture in the object plane, which defines the size, large or small, of an object, and acts as a source of diffraction. Its purpose is to limit the region over which microwaves reflect, or since we use the method of images, to limit the passage of microwaves from the effective (image) source through the object plane. The placement of the effective source is determined by the object curvature. For flat objects, the side of the object

towards the real source is extended so that it covers a plane, the object plane, then the real source is reflected through the plane along the line containing the real source and perpendicular to the plane. For distant real sources, this means a distant effective source, which will be important in our later discussion of parameter variation rates. A curved (spherical) object's effective source position is determined by the radius of curvature of the sphere R: when the source is a distance R_1 away from the reflector, the image is a distance $R_2 = R - R^2/(R_1+R)$ behind the sphere's surface [26]. Thus, the effective source is likely to be much closer to the calculation point when the object is curved than when it is not. The amplitude of each effective source is given by the reflectivity times a factor that is required to obtain the intensity of the source at the center of the reflector's aperture. Complex objects are represented as several flat or curved objects with adjacent apertures.

Now that we have calculated the position of the effective source for the n-th reflector, $\mathbf{r}_{effscatt,n}$, we can calculate its contribution to the electric field at the mobile's position, $\mathbf{r}_{ptat}$. The tips of the vectors are noted in the horizontal projection, Fig. 1, including the time dependent $\mathbf{r}_{ptat}$ that indicates the position of the mobile and brings time dependence into the equations below. The origin is arbitrary so is not shown in the figure. The Fresnel diffraction formalism with point-illumination [27] is used to calculate the field for each reflector in the region of interest. The interference pattern or flat fading coefficients c(t) (coherent sum of the complex electric fields $E_n(t)$ of wavelength) generated by N plane-wave reflectors with (time-dependent) parameters: amplitude A_n, (Doppler) frequency f_n and phase $_n$, and time averaged over an optical cycle, can be written as:

$$\text{Pattern} = c(t) = \sum_{n=1}^{N} E_n(t) = \sum_{n=1}^{N} A_n\, e^{-2\pi j f_n t + j\phi_n}, \qquad (1)$$

$$E_n(t) = \left[\frac{E_{in} e^{-2\pi j r/\lambda + j\phi}}{2} \frac{|\mathbf{r}_{scatt} - \mathbf{r}_{effscatt}|}{r} [C(w_{x2}) - C(w_{x1}) - jS(w_{x2}) + jS(w_{x1})][C(w_{y2}) - C(w_{y1}) - jS(w_{y2}) + jS(w_{y1})]\right]_n$$

with $w_{xm} = \sqrt{\frac{2}{\lambda \rho}}\,(x_m - x_0)$, $w_{ym} = \sqrt{\frac{2}{\lambda \rho}}\,(y_m - y_0)$, C and S the Fresnel integrals [27] and $\frac{1}{\rho} = \frac{1}{|\mathbf{r}_{scatt} - \mathbf{r}_{effscatt}|} + \frac{1}{|\mathbf{r}_{ptat} - \mathbf{r}_{scatt}|}$. All variables refer to the n-th reflector (the index is dropped in

the equation for clarity) with the exception of Γ and $\mathbf{r}_{ptat}$, which do not vary with n. All time dependence enters through $\mathbf{r}_{ptat}$ in Γ_n and r_n. The parameters and position vectors $\mathbf{r}_{scatt,n}$, $\mathbf{r}_{effscatt,n}$, $\mathbf{r}_{ptat}$, $x_{1,n}$, $x_{2,n}$ and $r_n = |\mathbf{r}_{ptat} - \mathbf{r}_{effscatt,n}|$ are defined in Figure 1. The reflector at $(\mathbf{r}_{scatt})_n$ has reflectivity ρ_n, and incident power from the transmitter $(E_{in})_n$. The phase factor, $e^{-2\Gamma j\tilde{r}/\lambda + j\phi}$, contains the propagation term proportional to $\tilde{r}_n$ and the phase from the reflection process, ϕ_n. It could also include effects from index variation due to thermal plumes, but we do not include them since their variation rate is slow so will not affect LRP performance. The propagation term $\tilde{r}_n$ is simply r_n for a flat reflector, but needs to be increased by $|\mathbf{r}_{trans} - \mathbf{r}_{scatt,n}| - (R_2)_n$ for a curved reflector since the placement of the effective source is closer to the aperture than the transmitter in this case. The phase ϕ_n could be calculated with the Fresnel formulae, [27], but we treat it as a constant. It depends upon the details of the object such as its complex index of refraction, and tends to slightly compress or expand the pattern, so its variations have the same effect as small changes in vehicle speed. We do not insert the spatial variation of this contribution to the phase. For clarity in this paper, we make the common 2d assumption [10] by taking an infinite aperture in the vertical-, y-direction. The Fresnel integral term for the y direction in square brackets reduces to $\sqrt{2}$.

To create a dataset, the user of the model specifies the location of the transmitter, $\mathbf{r}_{trans}$, and the centers of the apertures, $\mathbf{r}_{scatt,n}$, for each reflecting object. The aperture will typically be the size of the object itself, positioned on the side of the object towards the incoming radio waves. The orientation of the aperture, object reflectivity, object curvature, and reflection phase shift are also specified for each object. To allow for shadowing of the transmitter, an aperture can be specified for it (as is implicitly specified for the other reflectors by their size and location). The field calculation for the transmitter including its aperture is the same as that for the effective sources, except the transmitter position is specified and does not need to be calculated. Other inputs to the modeling program include the carrier frequency and region of interest (location, size and number of points for each of the two dimensions). The region of interest may be any rectangular array of points from a square to a single line in either direction. The model calculation running on a

Macintosh G3 computer takes a few seconds for several thousand points in the region of interest with ~10 reflectors, or a few minutes for ~100,000 points in the region of interest and ~100 reflectors.

Extensions of this model allow: (1) the calculation of the time delay profile [8, 9, 17] as a function of mobile position, by simply adding the delay of each path segment, from the transmitter to the reflector and the reflector to the mobile, so that the delay is $t_n = r_n/c$, with c the speed of light, (2) modeling of wideband signals, for which the algorithm is run at a set of frequencies, and (3) shadowing of reflected signals by intervening structures [17]. This is in addition to the above-noted transmitter shadowing, and is accomplished in an approximate manner by moving the aperture away from the object plane (i.e. assuming that the object's reflections are limited by the shadowing structure rather than the object size). When this is done, the object plane is used only to determine the location of the effective source.

III. Model Insights

The model insights derive from the simple relation between the field contribution from each component and the (effective) point source and aperture response in the model. For a specific example, consider one large flat and five curved reflecting objects creating an interference pattern with the source. The 1 GHz source is 105m to the left of the center of the 10m square region shown in Figure 2(a). A large object (building) 10 m to the right of the region does not run perpendicular to it, so its effective source is 130 m to the right of the region's bottom. Its amplitude reflection coefficient is 2/3. The five spherical reflectors to the right are evenly spaced on a 10 m long line as shown and with effective sources 1.8 m to the right. They approximate five cars parked along the road. The interference pattern (route 2) shown in Figure 2(b) is complex with narrow, deep fades which are ~1/100 the average power. The Doppler shifts f_n are easy to calculate as a function of position with the image method: for a stationary source (reflector) and v<<c, it is given by $f_n = f_c(v/c)\cos\theta_n$, where f_c is the carrier frequency, v is the speed of mobile (26.6 m/s here), c is

the speed of light, and θ_n is the incident angle of the Poynting vector (ray direction or wavefront normal) relative to the mobile's direction [8, 9]. The change in angle towards the effective source, which dominates the Doppler frequency variation rate for constant mobile velocity, is slow (< 18 Hz/second) for the reflection from the flat object, since the image source is distant. Conversely, the proximity of the effective sources for the curved objects causes faster variations. Route 2 in Figure 2(a) passes close to the curved objects, so those components of the interference pattern will have relatively rapid Doppler frequency variations (up to 890 Hz/second). This variation causes this route to be a challenging case, although the variation rate is still much slower than that of the channel c(t). The rate of Doppler frequency variation along route 1 is <200 Hz/second, which is more typical in practice. Other sources of change in the Doppler frequencies are due to changes in the mobile's speed and direction. These are on the seconds time scale unless there is an accident, so are not as limiting. The amplitudes, $A_n(t)$ in Eqn. 1, also vary more quickly along route 2, due to the 1/r dependence of Eqn. 1 and diffraction effects. Diffraction effects are important for small objects and reflections near the edges of larger objects. For a small object, the reflection (diffraction) has a well-defined maximum that spreads with characteristic angle approximated by x/r = λ/l_x radians for an object of size $l_x = (x_2-x_1)$.

In general, the insights gleaned from the model indicate that the variation of the amplitudes $A_n(t)$ and the Doppler shifts $f_n(t)$ are slow in space except near curved objects and near the edges of medium-sized flat objects and shadowing objects. The phase shifts ϕ_n do not vary except due to the Fresnel formula results mentioned above, or propagation conditions such as thermal plumes. Shadowing by a nearby building can also be challenging, resulting in the addition of a significant reflector in as little as 0.1 sec (derived from edge diffraction formulae as built into (1)), although this time increases linearly with the distance from the building. These events (passing near a car or shadowing by a nearby building) are short in duration and relatively rare.

IV. Understanding Measured Data Statistics

The long-range prediction method was tested with field-measured data to compare performance with the data sets produced with our model. The results are very similar to the model-based tests [1, 3, 17, 18]. The measured data was provided by Ericsson, Inc. and contained 100,000 samples taken at a sampling rate f_s = 1562.5 Hz, and at a carrier frequency f_c = 1877.5 MHz. The mobile speed during acquisition varied between 0 -> 50 km/hr, but most samples were taken at 30 km/hr. The sampling environment was low density urban Stockholm (Kista). The measurement system and environment are similar to those used in Ref. [28, 29, 30, 31].

We begin by showing that the measured data is indeed not stationary by comparing empirical autocorrelation functions from a few different segments of the data set[†][32]. This is shown in figure 3. These differences result from the variation in the number and locations of the reflectors along the measurement track. For example, one 10,000-point segment (sample points 55,000 ~ 65,000) of the data set had an autocorrelation function that resembles the autocorrelation of Jakes model with an infinite number of reflectors [8]. Another segment (samples 1 ~ 10,000) of the measured data had an autocorrelation function with a much wider main lobe and a flatter tail. Our goal here is to understand the types of environments that produce these various autocorrelation functions. In particular, will they be produced in environments that are dominated by distant effective sources, as would be the case when the objects are flat, or where curved or smaller objects cause the effective source to be much closer to the mobile's path? These experiments provided us with insights into the types of reflectors in those environments and therefore into the nature of flat fading and the expected prediction accuracy.

Two model scenarios were generated to identify the autocorrelation properties in two important limiting cases. We will find that they resemble the autocorrelation functions found in two of the measured data segments. In the first scenario (called the *local effective source environment*), we assume 8 curved reflectors are randomly and closely set along two sides of a 100 meter road,

[†] We define 'autocorrelation function' here and afterwards as the autocorrelation function for the observation samples in the empirical sense, not for a random process in the statistical sense.

illustrated in Figure 4(d). This scenario is expected when the mobile passes cars parked along the side of the road. In the second scenario (called the *remote effective source environment*), 8 flat reflectors have effective sources distant from the road, as shown in Figure 4(e). This scenario corresponds to buildings near the road, without parked vehicles. A remote effective image source does not imply a remote reflector, since the image source can lie far behind a flat reflector. We expect that the local effective aperture environment will be more common in urban or suburban areas, due to the larger number of cars, and that the remote effective source environment will be more common in rural areas and in industrial areas without street parking, but that the local/remote variation is probably more important than the urban/suburban/rural distinction for LRP performance. In both cases, the carrier frequency used was f_c = 1GHz, and the vehicle speed 49.68 km/ h, corresponding to a Maximum Doppler shift of 46 Hz. We modified the original data (both physical model datasets and the measured datasets) by subtracting the mean values and normalizing the average power to unity. These modified datasets were used throughout the paper. By examining the probability density functions (pdf) of fading coefficient amplitudes, we confirm that the distribution of this data is very close to Rayleigh fading for both channels, which can be seen in Figure 4(c).

The qualitative features of the local and remote effective source autocorrelation functions, the width of the primary peak, and sidelobe height can be understood from the model. In the discussion below, we assume that the vehicle speed, or equivalently the maximum Doppler shift, the maximum f_n, is fixed. The presence or absence of sidelobes depends largely on the balance between the period of oscillation of the interference pattern (related to the spread in angles of incidence of the components), and the distance over which non-stationarity effects become important (parameter variations). To see how the spread of angles affects the oscillation period, recall that co-propagating beams show no interference, while counter-propagating beams have a $\lambda/2$ oscillation period. The reflectors in the local effective source environment subtend a larger angle than those in the remote case, so one expects more closely spaced sidelobes for the local case, as is

seen in Figure 4(a). This suggests that data in Fig. 4(a) is from a region with a significant number of local reflectors, such as a region with cars along the road. The effects of non-stationarity depend upon the interval averaged over. In the interval we used to calculate the autocorrelation function for the remote case, the wider-spaced sidelobes have been reduced by the parameter variations (via oscillation period variations along the track).

The coherence time, or width of the primary autocorrelation peak, depends inversely on the range of Doppler frequencies present. It decreases with increasing angular range of the incoming wavefronts, so will be larger in the remote effective source environment, as seen in Figure 4(b). This suggests that distant effective sources, such as reflections from flat buildings along the road, dominate the signal in this segment. We have also found that it decreases with increasing dispersion of tilt angles for a set of flat (remote effective source) reflectors. The fading with the autocorrelation derived in Jakes' book [8] requires a large range of Doppler shifts, so has the shorter coherence time and large sidelobes. It resembles the local effective source environment or the circle of reflectors (large range of angles) in the Jakes model. This behavior could also result from remote effective sources when they are spread over a sufficiently large angular range. We note that one can concoct geometric placing of local effective sources so that the autocorrelation function has much smaller sidelobes than in Fig. 4(a) -- take a path so close (~1-2 m) to the effective sources that parameter variations wash out even the closely spaced sidelobes for any reasonable autocorrelation sampling length, but this is an unusual case. Through these comparisons, we conclude that the low density urban measured data was collected from regions with and without parked cars, and that these represent diverse mobile radio environments, which can be understood using our physical model.

V. Understanding Long Range Prediction Performance

A novel long-range linear prediction (LRP) method for the flat fading channel was proposed in [1, 4, 5]. It is different from the conventional channel estimation in two aspects. *First*, the novel LRP method focuses on predicting the future behavior of the fading coefficients rather than

estimating its current value. *Second*, in contrast to conventional channel estimation employed at high sampling rate (usually at the data rate, of ~20 kHz or higher, e.g. [33]), the novel method uses considerably lower sampling rate (on the order of twice the maximum Doppler frequency), which allows the long range channel behavior to be captured [1, 7]. Low rate samples are then interpolated to predict the channel coefficients at the data rate. The LRP method is based on autoregressive modeling. In this model, the predicted future channel sample $\hat{c}_n$ is based on p previous channel samples $c_{n-1}, \cdots, c_{n-p}$:

$$\hat{c}_n = \sum_{j=1}^{p} d_j c_{n-j} \tag{2}$$

where c_n is the fading signal c(t) in (1) sampled at the lower rate, p is the model order, and the optimal minimum mean square error (MMSE) coefficients d_j are determined by the orthogonality principle [1, 7].

Channel parameter variations and the limited initial observation interval necessitate adjustment of the LRP coefficients d_j in (2). These adjustments are performed as new channel samples are received. To update the LRP coefficients d_j's when the n-th channel sample becomes available, the least mean squares (LMS) adaptive tracking method assigns [34]:

$$\underline{d}(n+1) = \underline{d}(n) + \mu e_n \tilde{c}_n^*, \tag{3}$$

where μ is the step-size, $\underline{d}(n)=(d_1(n), \ldots d_p(n))^T$ is the time-dependent vector which reflects the variations of channel model parameters, $\underline{\tilde{c}}(n)=(\tilde{c}_{n-1}, \ldots, \tilde{c}_{n-p})^T$ is the vector of updated channel estimates, and the error signal, $e_n = c_n - \hat{c}_n \approx \tilde{c}_n - \hat{c}_n$. In this paper, we set $\tilde{c}_n = c_n$ in the computation of e_n and assume that noise-free channel samples c_n are observed. In [1, 7], we show how an estimate $\tilde{c}_n$ can be computed in the presence of noise using the decision-directed LMS algorithm. Improved adaptive tracking using recursive least squares (RLS) adaptation of the coefficients d_j was addressed in [17, 18]. Application of adaptive tracking significantly improves accuracy and provides robustness for long-range prediction as the physical channel parameters vary.

Since feedback and processing delay are inevitable, the prediction of several samples (several ms) ahead rather than just one step ahead, as (2), is usually desired. To achieve the long

range prediction, improved parameters $\underline{d}(n)$ are used in the modified iterative autoregressive equation to predict future channel samples [1, 3]

$$\hat{c}_{n+r} = \sum_{j=1}^{r-1} d_j(n+1)\hat{c}_{n-j+r} + \sum_{j=r}^{p} d_j(n+1)c_{n-j+r,}, \; r=1\ldots R, \tag{4}$$

where R is the prediction range. The $\hat{c}_{n+R}$ is the prediction of c_{n+R} R samples ahead. When delay exists, we cannot update all of the d_j in (4) until the corresponding actual channel samples become available. Thus, we have to use $\hat{c}_{n-j+r}$ for j=1, ···, r instead of using the actual c_{n-j+r} for j = r, ···, p in (4). Since the sampling rate is lower than the data rate, even R=1 implies prediction from tens to hundreds of data bits ahead. For example, in [7] the sampling rate is 500 Hz, and for R = 1 we predict 2 ms ahead. Prediction can be performed at the receiver or at the transmitter, depending upon computational complexity constraints. The feedback requirements are low in either case since the symbols need to be fed back only at the low sampling rate. If prediction is implemented at the receiver, feedback load can be reduced further for some adaptive transmitter applications. For example, only antenna selection bits for selective transmitter antenna diversity systems [1, 32], or only modulation level for adaptive modulation applications [1, 2] needs to be fed back.

We have previously shown the importance of using a nonstationary channel model for testing the prediction algorithm (prediction accuracy on Jakes model data is different from measured data) and that our model can produce datasets with realistic parameter variations (the prediction algorithm performance is similar to its performance on measured data) [1, 3, 17, 18]. This can also be observed in Fig. 5, for which the MSE = $E(c_n - \tilde{c}_n)^2$ at short prediction ranges (up to 0.3□) and saturation at larger prediction ranges is similar for the measured and physical model data, while being significantly different for the stationary Jakes model data. At short prediction lengths, fading generated by Jakes model is easier to predict due to stationarity, but at longer prediction intervals (more evident for prediction greater than a wavelength as in [17]), the measured data and physical model prediction MSEs saturate, while the MSE for the Jakes model prediction rises above them. This is probably due to the lower number of significant reflectors in reality compared to those (all at equal amplitude or importance) in the Jakes model.

We now show that the performance of the LRP algorithm in various environments can be explained using insights from our model. In all cases, the complex fading coefficients c(t) are predicted using the adaptive LRP algorithm jointly with LMS tracking of the autoregressive (AR) model coefficients as in equations (2-4) [1, 7]. Although the prediction method doesn't use them, the variations of Doppler shifts and amplitudes with position for each of the reflected components can be computed as discussed in section II, and can be used to explain the adaptive tracking performance. The MSE performance is compared for the typical vs. challenging cases using MSE vs. model order or prediction range. Figure 6 shows the geometry used and the results. We used randomly placed reflectors to the right of the region, constraining them to be near the path but at least a certain distance (for physical feasibility, see the figure) from the mobile's path. As the insights from the model suggest, the path closer to the effective sources is relatively more difficult to predict as measured with both metrics. We also find that the performance of the prediction algorithm is adequate even for the challenging case, validating its performance in diverse environments.

Finally, we show that the insights identifying challenging and typical cases apply to signaling via bit error rate (BER) simulations. In [1, 7] we applied the long-range prediction algorithm to study adaptive transmission techniques as selective transmitter diversity and adaptive modulation. To demonstrate the application of the proposed prediction method for adaptive power control, we analyzed the Truncated Channel Inversion algorithm (TCI) [2] aided by long-range prediction (see also [5, 6, 7]). The underlying theme of this scheme is to interrupt transmission for time intervals when the predicted power level is below a previously chosen threshold value, th, and send the data symbols scaled by the inverses of the predicted fading coefficients when the predicted power is above the threshold. In simulation, we used binary phase shift keying (BPSK) as the modulation scheme, and assumed coherent detection. The reflecting object environment used to create the typical and challenging case fading resembles the one shown in Figure 2(a), except the large reflector is removed (to reduce the effect of LOS) and 14 curved reflectors are randomly placed along the right side of the 100 meter road. The fading signals generated along the equivalent

of routes 1 and 2 in Figure 2 (a) are considered as typical and challenging cases, respectively. The channel sampling rate is 1000 Hz and the Maximum Doppler shift 67 Hz, corresponding to a vehicle speed of 45 miles /h for f_c = 1 GHz. The data rate is 50 Kbps. The simulation utilized 2-step (2 ms) ahead prediction. The BER performance is illustrated in Figure 7. The performance difference shows that our physical model insights can help us create different mobile radio environments that both test the limits of our prediction method and validate its application in adaptive power control, for a range of environments.

VI. Conclusions

We have described a physical model that generates realistic, *non-stationary* data for testing the algorithm for long-range prediction of wireless signals, and *provides expectations* of the degree of prediction difficulty for various environments. This physical model can be used to gain insights into the interference patterns that give rise to multipath fading in mobile communications. It allows calculation of the rate at which reflected components' amplitudes and frequencies vary, and hence the adaptive tracking speed required to accurately predict future channel properties. The parameters vary slowly enough for tracking in most cases, on the order of 0.1 second even in challenging cases. This is much slower than the variation rate of the actual fading channel. The model can be used to determine the nature of the environments in which measured data were acquired via channel statistics, and can be used to test channel prediction methods. The important messages are that prediction is tractable, our physical model correctly identifies typical and challenging scenarios as measured by MSE performance of the LRP algorithm, the MSE performance when measured data is used is similar to that when our model is utilized to generate the channel, and the prediction algorithm has acceptable performance even in very difficult scenarios. We couldn't assert the last statement without the model insights.

Acknowledgement

The authors would like to thank Jan-Eric Berg and Henrik Asplund of Ericsson, Inc. for providing the measurement data set.

References

[1] A. Duel-Hallen, S. Hu, H. Hallen, "Long-range Prediction of Fading Signals: Enabling Adaptive Transmission for Mobile Radio Channels", *IEEE Signal Processing Magazine*, Vol. 17, No.3, pp. 62-75, May 2000.

[2] A. J. Goldsmith and S. G. Chua, "Variable-Rate Variable-Power MQAM for Fading Channels", *IEEE Trans. Commun.* , vol. 45, No. 10, pp. 1218 - 1230, Oct. 1997.

[3] S. Hu, H. Hallen and A. Duel-Hallen, "Physical Channel Modeling, Adaptive Prediction and Transmitter Diversity for Flat Fading Mobile Channels," *Proceedings of SPAWC'99*, May 1999, pp.387-390.

[4] T. Eyceoz, A. Duel-Hallen, and H. Hallen "Prediction of Fast Fading Parameters by Resolving the Interference Pattern", *Proceedings of the 31st ASILOMAR Conference on Signals, Systems, and Computers*, Nov. 2-5, 1997.

[5] T. Eyceoz, A. Duel-Hallen, H. Hallen, "Deterministic Channel Modeling and Long Range Prediction of Fast Fading Mobile Radio Channels," *IEEE Commun. Lett.,* Vol. 2, No. 9, pp. 254 – 256, Sept. 1998.

[6] S. Hu, H. Hallen and A. Duel-Hallen, "Adaptive Power Control Using Long Range Prediction for Realistic Fast Fading Channel Models and Measured Data", *5th International Symposium on Communication Theory and Application ISCTA'99*, July,1999, pp.118-120.

[7] T. Eyceoz, S. Hu, and A. Duel-Hallen, "Performance Analysis of Long Range Prediction for Fast Fading Channels", *Proc. 33rd Annual Conference on Information Sciences and Systems CISS'99*, March 1999, Volume II, pp.656-661.

[8] W. C. Jakes, Jr., *Microwave Mobile Communications*. New York: Wiley, 1974.

[9] T. S. Rappaport, *Wireless Communications: Principles and Practice*, Prentice Hall, 1996.

[10] R.B. Ertel, P. Cardieri, K.W. Sowerby, T.S. Rappaport, J.H. Reed, "Overview of spatial channel models for antenna array communication systems," IEEE Personal Communications, Volume: 5 Issue: 1 , Feb 1998, pp. 10 -22.

[11] U. Dersch, "Physical modelling of macro, micro and inhouse cell mobile radio channels," Third IEEE International Symposium on Personal, Indoor and Mobile Radio Communications, 1992. Proceedings, PIMRC '92, 19-21 Oct 1992, pp. 64 –68.

[12] Ming Lu. T. Lo, J. Litva, "A physical spatio-temporal model of multipath propagation channels," Vehicular Technology Conference, 1997 IEEE 47th , Volume: 2 , 4-7 May 1997, pp. 810 –814.

[13] A. Saleh, R. Valenzuela, "A Statistical Model for Indoor Multipath Propagation," IEEE Journal on Selected Areas in Communications, Volume: 5 Issue: 2 , Feb 1987, pp. 128 -137.

[14] Q.H. Spencer, B.D. Jeffs, M.A. Jensen, A.L. Swindlehurst, "Modeling the statistical time and angle of arrival characteristics of an indoor multipath channel," IEEE Journal on Selected Areas in Communications, Volume: 18 Issue: 3 , Mar 2000, pp. 347 -360.

[15] T. Svantesson, "A study of polarization diversity using an electromagnetic spatio-temporal channel model," Vehicular Technology Conference, 2000. Fall VTC 2000. 52nd, Volume: 1, 2000, pp. 79 -86.

[16] W.R. Braun, U. Dersch, "A physical mobile radio channel model," IEEE Transactions on Vehicular Technology, Volume: 40 Issue: 2 , May 1991 pp. 472 –482.

[17] H. Hallen, A. Duel-Hallen, S. Hu, T.-S. Yang, and M. Lei, "A Physical Model for Wireless Channels to Provide Insights for Long Range Prediction," Proceedings of *MILCOM'02*, Anaheim, CA, Oct. 7-10, 2002, vol. 1, pp. 627-31.

[18] H. Hallen, S. Hu, M. Lei and A. Duel-Hallen, "A Physical Model for Wireless Channels to Understand and Test Long Range Prediction of Flat Fading," Proceedings of WIRELESS 2001, Calgary, Canada, July 9-11, 2001, pp. 99-107.

[19] B.H. Fleury, P.E. Leuthold, "Radiowave propagation in mobile communications: an overview of European research," IEEE Communications Magazine, February, 1996, pp. 70 –81.
[20] T. A. Russell, C. W. Bostian, and T. S. Rappaport, "A deterministic approach to predicting microwave diffraction by buildings for microcellular systems," *IEEE Trans. on Ant. and Prop.* vol. 41, no. 12, pp. 1640-9, Dec. 1993.
[21] M. Dottling, A. Jahn, J. Kunisch and S. Buonomo, "A versatile propagation channel simulator for land mobile satellite applications," Proceedings of VTC '98. 48th IEEE Vehicular Technology Conference. Pathway to Global Wireless Revolution, IEEE New York NY USA, 1998, pp. 213-217 vol.211.
[22] G. E. Corazza, V. Degli-Esposti, M. Frullone, G. Riva, "A Characterization of Indoor Space and Frequency Diversity by Ray-Tracing Modeling," IEEE Journal on Selected Areas in Communications, Vol. 14, No. 3, pp.411-419, April 1996.
[23] C. Tzaras, S. R. Saunders and B. G. Evans, "A physical-statistical time-series model for the mobile-satellite channel," Proceedings of 1998 IEEE APS Conference on Antennas and Propagation for Wireless Communications, IEEE New York NY USA, 1998, pp. 1-4.
[24] P. A. Mathews and B. Mohebbi, "Direction of arrival and building scatter at UHF", *Proc. 7th International Conference on Antennas and Propagation*, York, U.K., pp. 147-150, 1991.
[25] D.W. Browne, J. Medbo, H. Asplund, Jan-Erik Berg "A simple approach to site sensitive modeling of indoor radio propagation," Vehicular Technology Conference, VTC Spring 2002. IEEE 55th, Volume: 1 , 2002 Page(s): 384 –388.
[26] David Griffiths, Introduction to Electrodynamics, Prentice Hall, Englewood Cliffs, NJ 1981, p. 110.
[27] R.D. Guenther, *Modern Optics*, New York, Wiley, 1990.
[28] J.-E. Berg, "Building penetration loss at 1700 MHz along line of sight street microcells," Third IEEE International Symposium on Personal, Indoor and Mobile Radio Communications, 1992. Proceedings, PIMRC '92, 19-21 Oct 1992 pp. 86 –87.
[29] J.-E. Berg, R. Bownds, F. Lotse, "Path loss and fading models for microcells at 900 MHz," Vehicular Technology Conference, 1992 IEEE 42nd, 10-13 May 1992, pp. 666 –671.
[30] F. Lotse, J.-E. Berg, U. Forssen, P. Idahl, "Base station polarization diversity reception in macrocellular systems at 1800 MHz," Vehicular Technology Conference, 1996. 'Mobile Technology for the Human Race'., IEEE 46th, Volume: 3, 28 Apr-1 May 1996, pp. 1643 –1646.
[31] F. Harrysson, J.-E. Berg, "Propagation prediction at 2.5 GHz close to a roof mounted antenna in an urban environment," Vehicular Technology Conference, VTC 2001 Fall, IEEE 54th, Volume: 3, 2001, Pages: 1261 –1263.
[32] S. Hu, *Realizing the Potential of Adaptive Transmission Techniques Through Long Range Prediction for Fast Fading Mobile Radio Channels*, PhD thesis, North Carolina State University, 2000.
[33] Y. Liu and S. D. Blostein, "Identification of Frequency Non-selective Fading Channels Using Decision Feedback and Adaptive Linear Prediction," *IEEE Trans. on Commun.*, Vol. 43, No. 2/3/4, pp. 1494 – 1492, Feb./March/April 1995.
[34] M. H. Hayes, *Statistical Digital Signal Processing and Modeling*, John Wiley & Sons, Inc. 1996.

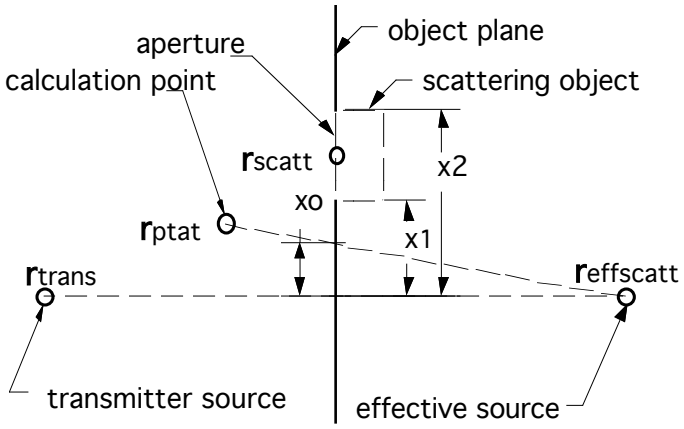

Figure 1. The parameters used to calculate the amplitude from one reflecting object, shown as a dotted rectangle. Also shown is the aperture chosen. The origin is arbitrary since only differences between the vectors are used. The x-direction shown here is defined for the particular object plane, and varies in direction for different objects; the y-direction is similar.

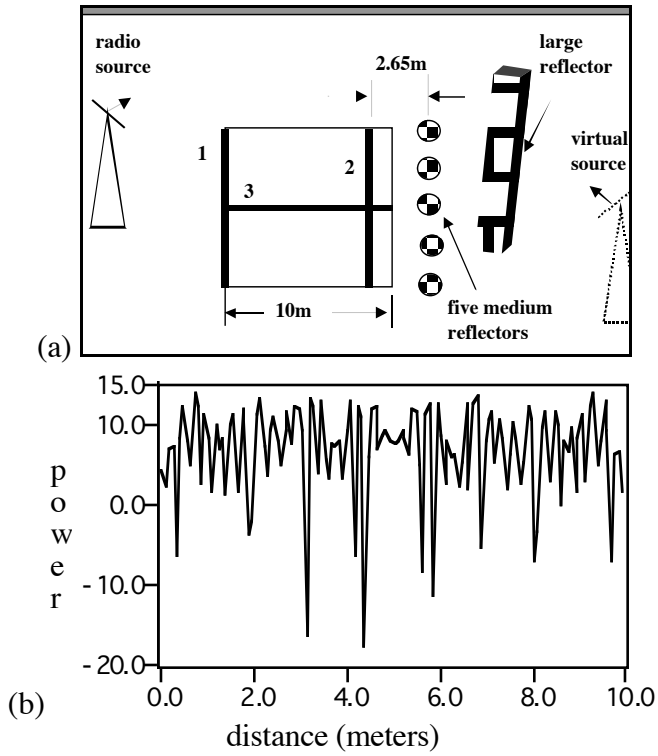

Figure 2 (a) Geometry used for the physical channel model calculation, with one large and five curved reflecting objects. (b). Line cut from the region shown in (a) (route 2, in dB with arbitrary zero). Divide the abscissa by the mobile's speed to get time.

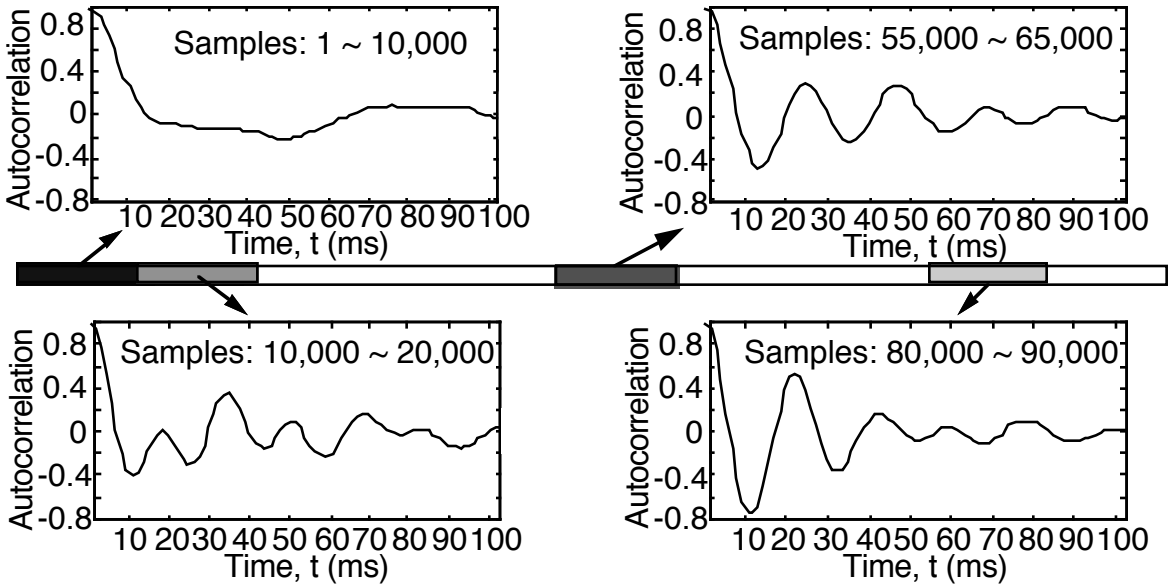

Figure 3 Empirical autocorrelation functions for various segments of the measured data, as indicated by the bar in the middle of the figure representing the entire data set. The variation indicates that the data is not stationary. The abscissa can be converted to distance by multiplying by the mobile's velocity, 30 km/hr.

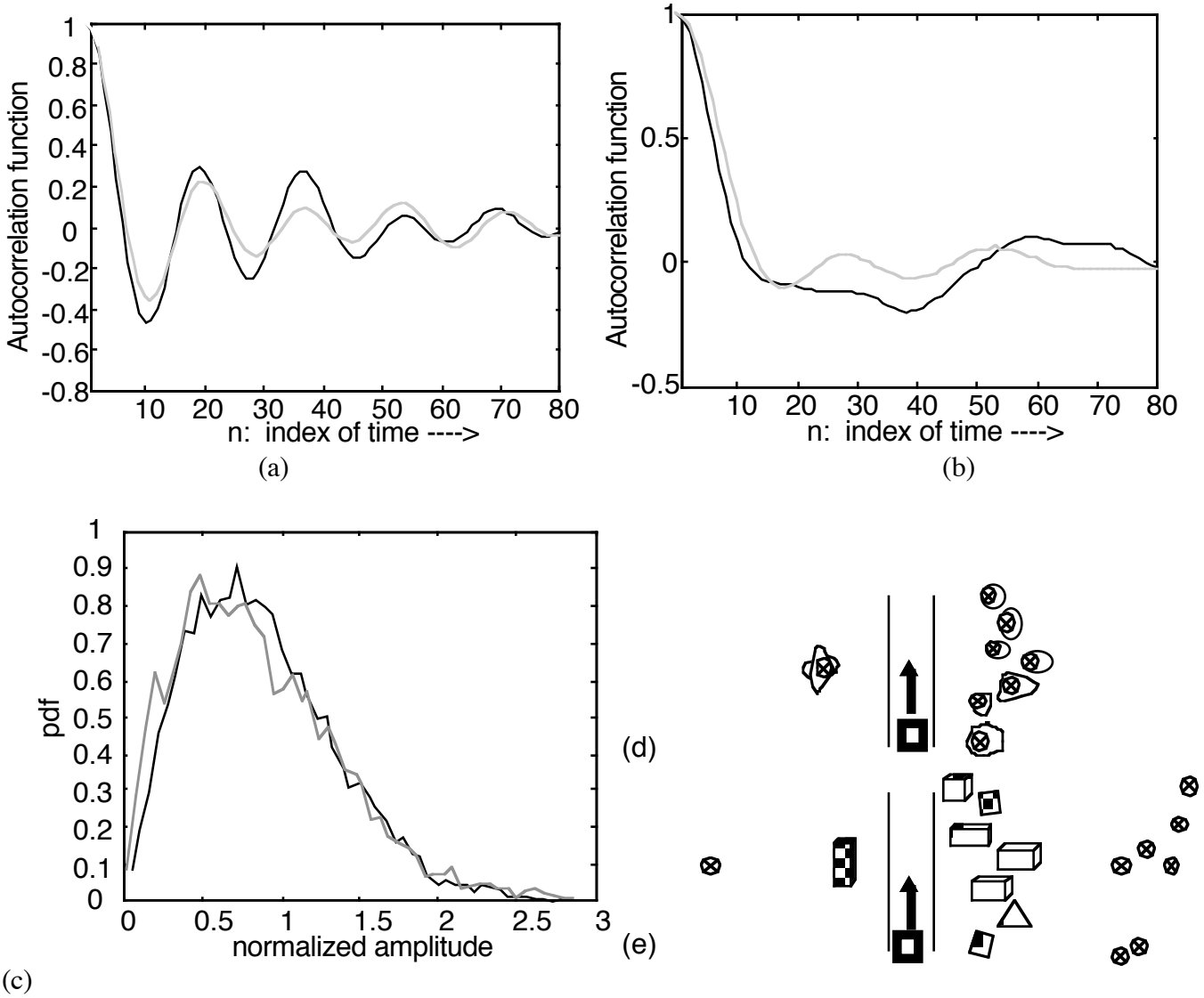

Figure 4. Comparison of the autocorrelation functions and pdf's of the physical model and measured data. Black: measured data; Light gray: physical model. (a): autocorrelation function for the local environment; (b): autocorrelation function for the remote environment; (c): pdf in the local effective source environment (similar to the pdf for the remote effective source environment); (d): local effective source environment. The reflectors are objects, the effective sources are circled x's; (e): remote effective source environment.

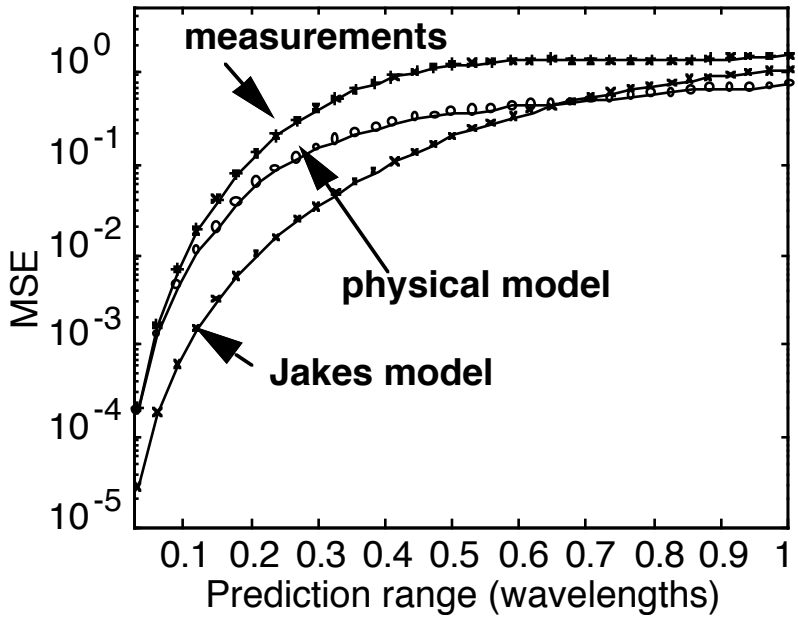

Figure 5. Mean square error of the prediction for Jake's model, physical data and measured data are given as a function of prediction range in wavelengths. (p = 40, the maximum Doppler shift f_{dm} = 46 Hz, and the sampling rate is 1562.5 Hz).

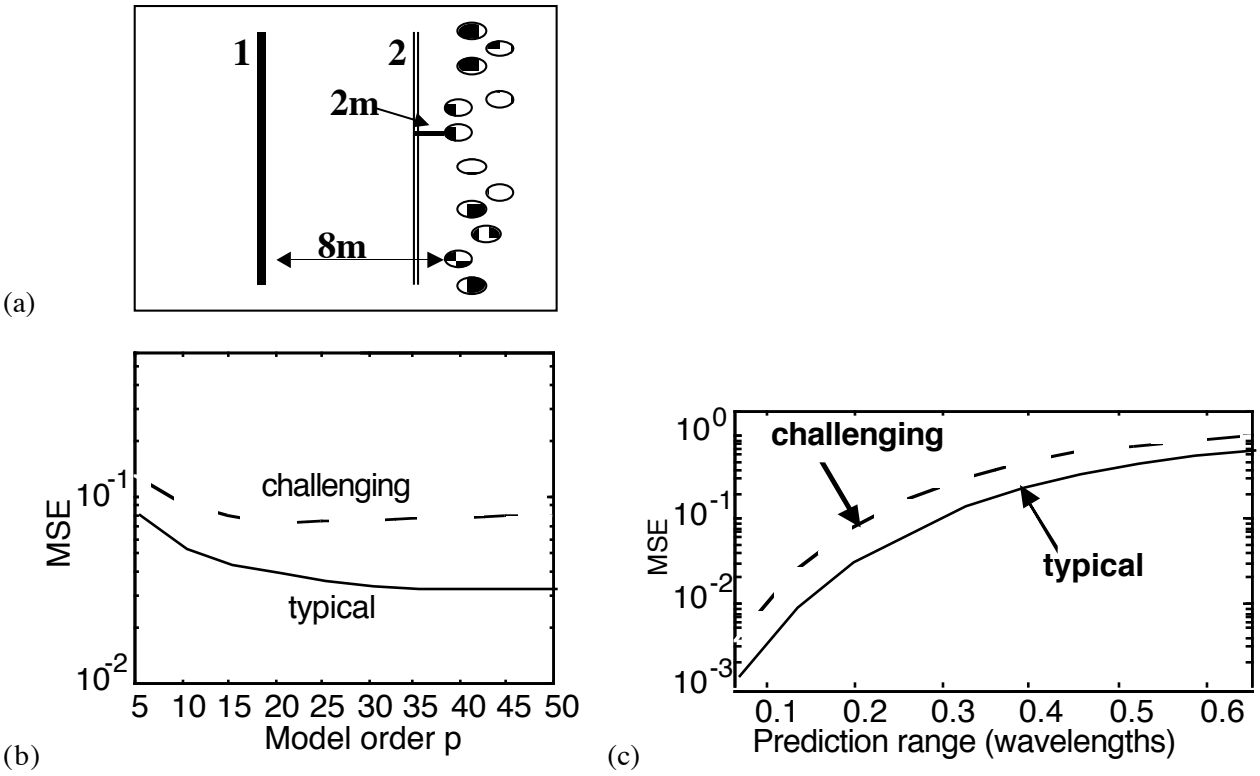

Figure 6. The mean square error of the prediction algorithm demonstrates that the challenging cases are more difficult to predict than the typical one, i.e. the insights apply, although the prediction is adequate for both cases. (a) The geometry shows the two paths and 14 curved reflectors randomly placed along the right side. The challenging case is within 2 m of the effective sources while the typical case is at least 8 m from them. A 1 GHz carrier frequency and 67 Hz maximum Doppler shift (45 MPH) are used with a 1 kHz sampling rate. (b) The MSE for the prediction vs. model order for 3 ms ahead prediction. (c) The MSE vs. prediction range for a model order p = 40.

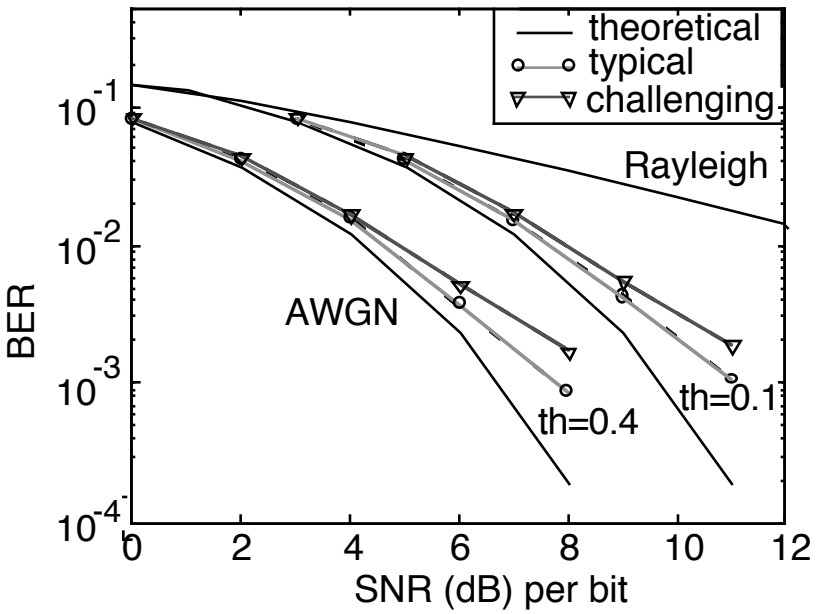

Figure 7. BER performance of TCI for typical and challenging case mobile radio environments is compared. Also shown are the theoretical limiting cases of Rayleigh fading and the average white Gaussian noise channel (AWGN). (2ms ahead prediction, f_{dm}=67Hz)